

Experimental Comparison of Rapid Large-area Direct Electron Beam Exposure Methods with Plasmonic Devices

Akio Higo,^{1*} Tomoki Sawamura,² Makoto Fujiwara,¹ Eric Lebrasseur,¹
Ayako Mizushima,¹ Etsuko Ota,¹ and Yoshio Mita^{1,2**}

¹VLSI Design and Education Center (VDEC), The University of Tokyo,
2-11-16 Yayoi, Bunkyo-ku, Tokyo 113-0032, Japan
²Graduate School of Engineering, The University of Tokyo,
3-7-1 Hongo, Bunkyo-ku, Tokyo 113-8656, Japan

(Received May 23, 2019; accepted July 25, 2019)

Keywords: electron beam lithography, character projection, variable-shaped beam, nanopatterns, color filter

We have quantitatively investigated a periodic nanostructure exposure process by electron beam lithography (EBL). The targeted applications are nano- to micro-electromechanical systems (NEMS/MEMS), nanophotonics, surface plasmonic structures, and metamaterials. It is confirmed that the character projection (CP) method can obtain both high throughput and high resolution simultaneously as compared with the variable-shaped beam (VSB) method. We used square, triangular, and octagonal CP stencil masks to realize a nanohole array (NHA) of 10.4 mm² area. The holes were placed in both square and hexagonal grid configurations. We measured the hole patterns by scanning electron microscopy (SEM) and scanning probe microscopy (SPM). Also, the effect of NHA size variation was measured on the basis of optical absorption spectra obtained using a system consisting of an optical microscope and a spectrum analyzer. The spectrum variation was confirmed to be in good agreement with the local size variation; identically fabricated NHAs showed identical spectra. It is therefore possible to control the nanometric critical dimensions by using NHAs as process indicators.

1. Introduction

Electron beam lithography (EBL) is an essential research and development tool for recent very large scale integrated circuits (VLSI), nano- to micro-electromechanical systems (NEMS/MEMS), nanophotonics, surface plasmonic structures, and metamaterials. To bridge the gap from research to industrial use, manufacturers require both high throughput and high resolution for lithography. If a high-throughput EBL technology with wafer-level patterning is achieved, a new production scheme with a short turnaround time and a high degree of design flexibility will be realized. Towards this end, high-throughput EBL methods have been developed. One method is the variable-shaped beam (VSB) method. As shown in Fig. 1(a), the VSB method

*Corresponding author: e-mail: higo@if.t.u-tokyo.ac.jp

**Corresponding author: e-mail: mita@if.t.u-tokyo.ac.jp

<https://doi.org/10.18494/SAM.2019.2443>

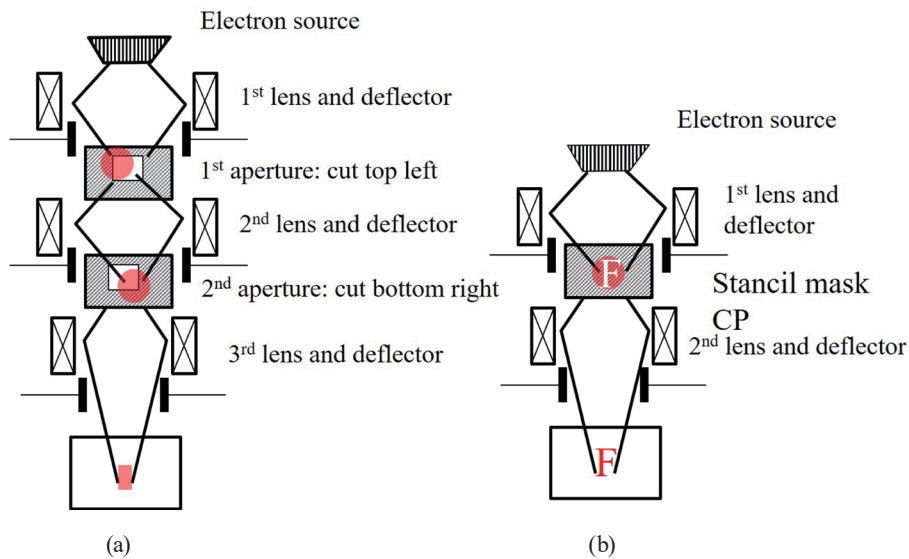


Fig. 1. (Color online) General high-throughput EB exposure methods: (a) variable-shaped beam (VSB) and (b) character (or cell) projection (CP) methods.

uses size-variable rectangular electron beam (EB) patterns instead of the Gaussian-shaped beam used in classical machines. The VSB method is compatible with the traditional LSI design employing rectangular devices and orthogonal connections. An alternative is the character (or cell) projection (CP) method. As shown in Fig. 1(b), stencil mask patterns preinstalled in the machine are used instead of VSB rectangles. The CP and VSB methods can be combined to draw larger patterns such as optical race tracks.^(1,2)

Since the 2000s, such new technology has become accessible at open platforms such as nanotechnology platform nanofabrication sites. In 2019, two nanofabrication sites at Kyoto University and The University of Tokyo (UTokyo) providing EBL facilities employing the VSB and CP methods were opened to the public for R&D. The UTokyo Nanofabrication site, operated by VLSI Design and Education Center (VDEC) in collaboration with the School of Engineering, consists of a total of 600 m² of cleanrooms of U.S. Federal classes 1, 100, 1000 Super Cleanroom (SCR) located in the Takeda Sentanchi Building. Two EBL systems are available for direct chip, 2 to 8 inch wafer, and 5 inch photomask writing. One EBL system is an ADVANTEST F5112-VD01 system installed in 2004, which supports the VSB method. The other is an ADVANTEST F7000S-VD02 system installed in 2013, which supports both the CP and VSB methods. Through the open use of these systems, we have experimentally found that new applications such as photonic and surface plasmon devices, and metamaterials require not only rectangular patterns but also precise nanometer-scale patterns such as circles and triangular shapes. The users of these systems critically require smooth pattern edges for realizing high device quality. To achieve such “ideal” shapes, the VSB method needs a number of very small rectangular shots with a rectangle height of as small as 10 nm, as shown in Fig. 2(b). Therefore, the exposure time is greatly increased. Increasing the rectangle height in the

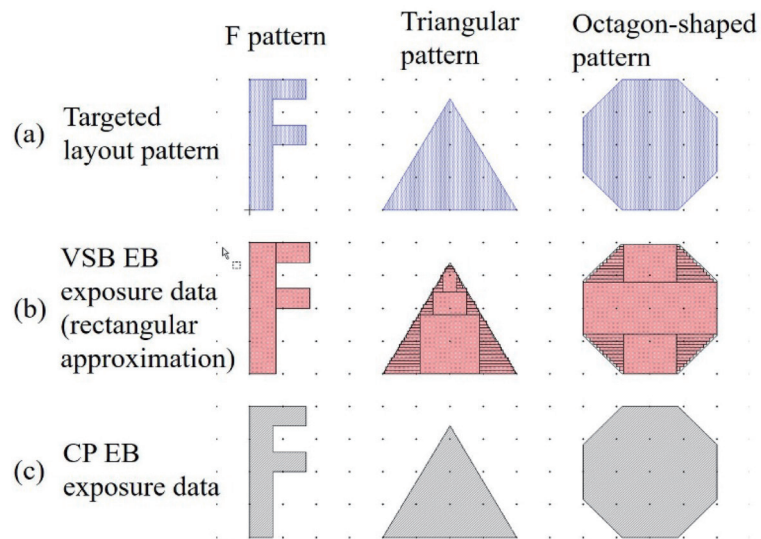


Fig. 2. (Color online) (a) Target patterns and examples of pattern approximation by (b) VSB and (c) CP methods.

VSB method results in pixel-like artifacts on oblique and curved edges. Such artifacts degrade device performance. In contrast, the CP method can be used for the single-shot exposure of stencils regardless of the complexity of the pattern, thus, achieving both a high throughput and a fine shape. For this reason, an increasing number of researchers are now using the CP method.

Evaluating the pattern quality is equally important as exposure. The standard evaluation methods are used for measurement by scanning electron microscopy (SEM) and scanning probe microscopy (SPM) techniques such as atomic force microscopy. Although these methods can be used to directly measure drawn structures, some problems exist such as artifacts due to charge-up and a tradeoff between the resolution and the observation area. As a method of simultaneously obtaining measurements and local shape quality information over a large area, we proposed an optical measurement technique for nanohole array (NHA) test structures^(3–9) as shown in Fig. 3. The extraordinary optical transmission (EOT) phenomenon occurs through an NHA; the light of a certain wavelength tunnels to the other side of the surface through holes as a result of the light coupling to the surface plasmon.

In this study, we investigated the NHA fabrication process in terms of throughput and pattern quality using F7000S-VD02. NHA arrays having several different hole shapes, sizes, placement lattice configurations, and distances were designed and fabricated on a 40-nm-thick aluminum thin film on a 525- μm -thick quartz substrate. The NHA was exposed to VSB and CP and the pattern variations due to the exposure and proximity effect correction (PEC) were compared by SEM, SPM, and optical color profile measurement.

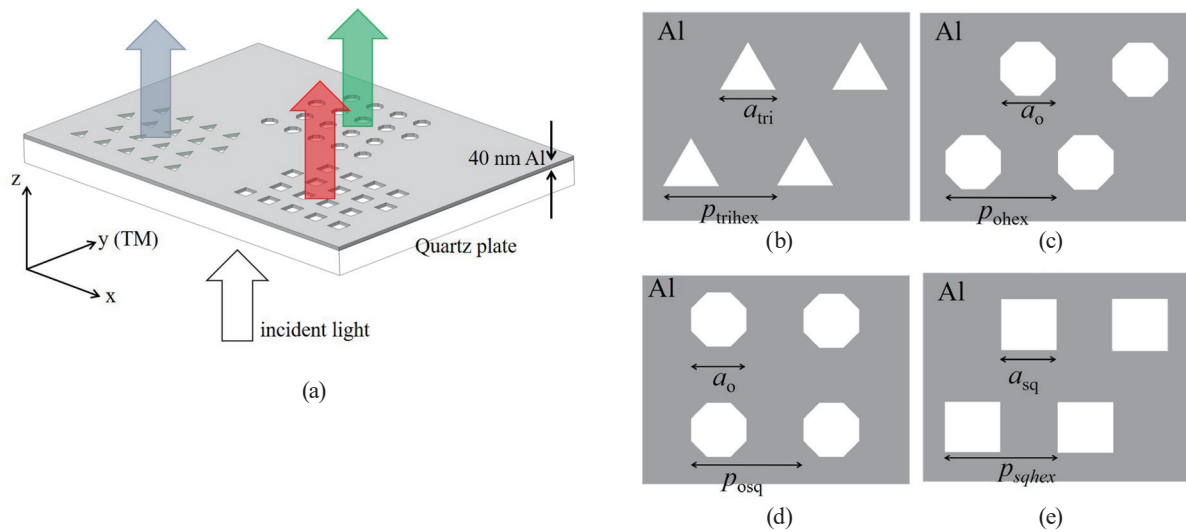


Fig. 3. (Color) Design of Al surface plasmon filter: (a) Al surface plasmon color filter, (b) hexagonal array of triangular holes, (c) hexagonal array of octagonal holes, (d) square array of octagonal holes, and (e) hexagonal array of square holes.

2. NHA Test Structure Design

2.1 Design and pattern conversion of NHAs

We designed a periodic nanostructure with triangular, octagonal, and square holes using computer-aided design (CAD) software. The patterns were exported to graphic database system II (GDSII) stream format data and then converted into the format accepted by our EB machine (BEF20 format for the F7000S-VD02 EB writer) using conversion software (GenISys Beamer⁽¹⁰⁾). The sizes of the triangular (a_{tri}), octagonal (a_o), and square (a_{sq}) holes were varied from 50 to 270 nm with a pitch of 10 nm. The period of each array (p_{trihex} , p_{ohex} , p_{osq} , p_{sqhex}) was twice the hole size ($2a_{tri}$, $2a_o$, $2a_o$, $2a_{sq}$) (see Fig. 3). The shapes had a one-to-one relationship with the corresponding CP stencil pattern; the 200 nm square was composed of a 2×2 array of 100 nm square CP patterns. The same patterns (triangular, octagonal, and square holes) were also composed of rectangles with a height of 10 nm in the VSB method.

During the conversion, PEC^(11,12) was also considered. When fabricating a mixture of micro- and nanopatterns, EB scattering in both the forward and backward scattering processes must be taken into account. The dose of each nanopattern depends on the size of the structure and its periodicity; therefore, PEC is indispensable when various periodic structures are exposed simultaneously. PEC was performed using the same conversion software (Beamer). PEC resulted in a dose ratio of 1.3 between the edge and the center of the exposure area for patterns with the 200-nm-size, 400-nm-pitch square holes, octagonal hole hexagonal array, and octagon hole square array. The 200-nm-size, 400-nm-pitch triangular holes with PEC had a dose ratio of 1.44. Four sets of converted patterns on the same substrate were exposed to CP or VSB for conversion with or without PEC.

2.2 Shot number and exposure time comparison between CP and VSB methods

We estimated and compared the shot number exposure time over a $10 \times 10 \text{ cm}^2$ area for octagonal and triangular holes by the VSB and CP methods. To expose octagonal and triangular hole patterns of 200 nm size, the total shot number reduction ratios of CP/VSB were calculated to be 0.077 and 0.056, respectively. On the one hand, the total CP shot numbers were identical to the hole numbers in the CAD design. On the other hand, to realize an oblique shape with the VSB method, the software converted the pattern into many thin rectangles; therefore, the shot number was larger for triangles (because the pattern contains only oblique shapes) than for octagons (because the pattern includes large rectangles). The exposure times of octagonal and triangular holes in the VSB method for a $10 \times 10 \text{ cm}^2$ area were estimated to be 1152230 s (approximately 320 h) and 1575920 s (approximately 437 h), respectively. In contrast, the exposure times of octagonal and triangular holes in the CP method were estimated to be 174432 s (approximately 48 h) and 175900 s (approximately 48 h), respectively. The exposure time reduction ratios of CP/VSB for octagonal and triangular holes were 0.15 and 0.11, respectively. In conclusion, the CP method can reduce the exposure time by a factor of 6 to 9.

3. Experiment and Discussion

3.1 Aluminum NHA fabrication

Aluminum was chosen for the simplicity of the process. We fabricated Al NHAs by the following procedure: 40-nm-thick $\text{Al}_{0.99}\text{Si}_{0.01}$ was sputtered onto a 525- μm -thick, 4-inch quartz wafer using an ULVAC SIH-450 system. EB resist (ZEP-520A-7) was spin-coated at 6000 rpm for 60 s to a thickness of 200 nm. The arrays were exposed to CP or VSB at a standard dose of $105 \mu\text{C}/\text{cm}^2$ at 50 kV. The machine used for exposure (F7000S-VD02) divided the total dose by a factor of three ($35 \mu\text{C}/\text{cm}^2$ each) and exposure was performed three times (so-called three-pass writing) to avoid excess heating and possible resist evaporation in the chamber (prone to contamination) resulting from high-current, high-dose exposure on a glass substrate. The sample was developed in a standard developer (ZED-N50) for 60 s and rinsed twice in ZED-B. The hole patterns were transferred to Al by inductively coupled plasma reactive ion etching (ICP-RIE, ULVAC NE-550) under the following conditions: an ICP coil radio frequency (RF) power of 400 W, a substrate bias power of 50 W, 15 sccm Cl_2 gas, 15 sccm BCl_3 gas, an etching pressure of 0.5 Pa, and heat transfer tape pasted on a silicon carrier wafer. The etching rate of Al was 300 nm/min. After etching, the resist mask was removed by an EB resist remover (ZDMAC) on a hot plate at 80 °C.

3.2 Microscopy observation

We observed the sample with a microscope (STM6, Olympus Corp.) as shown in Fig. 4. Photographs were taken with a digital camera (D5300, Nikon Corp.) attached to the microscope with the sample illuminated from underneath with the light bulb of the microscope. The NHA

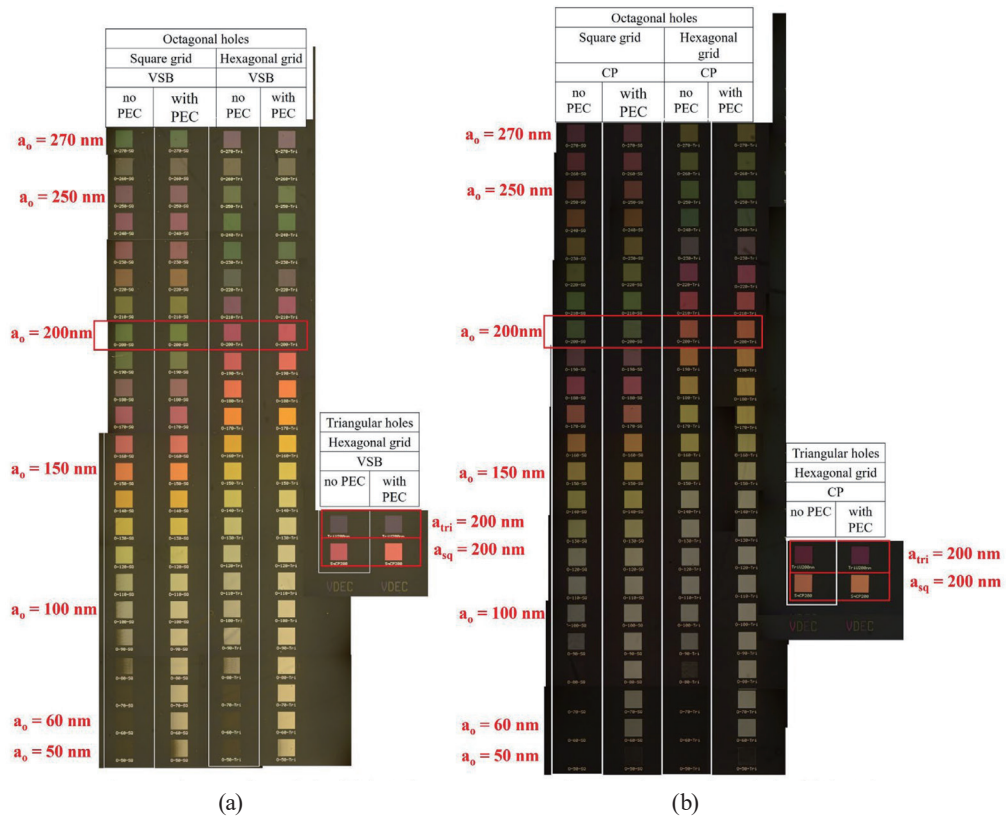








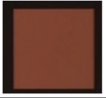
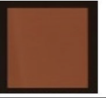


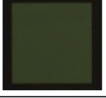
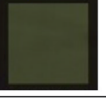
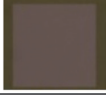
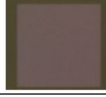
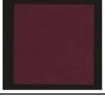

Fig. 4. (Color) Transmission images of fabricated nanopatterns with measured samples in red-line rectangles: (a) VSB and (b) CP methods.

size was smaller than the wavelength of visible light transmitted for NHAs as small as 50 nm. Depending on the hole shape, size, placement, and conversion method, different colors were observed.

Among the 23 different hole sizes in Fig. 4, we investigated the $a = 200$ nm samples in detail. We define a unique ID number using the following notation: (hole shape)-(hole placement)-(conversion). The hole shape is either square (SQ), octagonal (O), or triangular (Tri). The hole placement is either a square (sq) or hexagonal (hex) grid. The conversion modes are VSB without PEC (VSB), VSB with PEC (VSBPEC), CP without PEC (CP), and CP with PEC (CPPEC). For example, the ID of square holes in a hexagonal grid fabricated by the VSB method without PEC is SQ-hex-VSB.

Table 1 shows a summary of the microscopy images of light transmitted through each pattern. Two observations can be made: (1) The color is uniform throughout the pattern area ($200 \times 200 \mu\text{m}^2$), thereby indicating uniform exposure and etching. (2) The patterns may have the same or different colors, depending on the conversion method of the VSB, VSBPEC, CP, and CPPEC methods. An effect of the submicron-scale pattern shape and size is suggested.

Table 1
(Color) Transparent color image of each pattern. The square size is $200 \times 200 \mu\text{m}^2$.

	VSB		CP	
	without PEC	with PEC	without PEC	without PEC
200nm square holes hexagonal grid	ID: SQ-hex-VSB 	ID: SQ-hex-VSBPEC 	ID: SQ-hex-CP 	ID: SQ-hex-CPPEC 
200nm octagonal holes hexagonal grid	ID: O-hex-VSB 	ID: O-hex-VSBPEC 	ID: O-hex-CP 	ID: O-hex-CPPEC 
200nm octagonal holes square grid	ID: O-sq-VSB 	ID: O-sq-VSBPEC 	ID: O-sq-CP 	ID: O-sq-CPPEC 
200nm triangular holes hexagonal grid	ID: Tri-hex-VSB 	ID: Tri-hex-VSBPEC 	ID: Tri-hex-CP 	ID: Tri-hex-CPPEC 

3.3 Absorption spectrum measurement

To quantitatively analyze the NHA optical property, absorption spectra were measured. As shown in Fig. 5(a), optical measurement was performed using a system consistency of an optical microscope (BX50, Olympus Corp.) and a spectrometer (FLAME-S, Ocean Optics Inc.) with an optical fiber attached. Both transmission and reflection spectra were taken. First, the transmission intensity spectrum of an NHA, $I_{NHA}(\lambda)$, the “open” transmission spectrum of quartz, $I_{open}(\lambda)$, the reflection spectrum of the NHA, $I_{rNHA}(\lambda)$, and the reference reflection spectrum $I_{short}(\lambda)$ of thick aluminum on a quartz were obtained, and the background was subtracted. Then, the normalized transmission and reflection spectra were calculated for all wavelengths using $\eta_t(\lambda) = I_{NHA}(\lambda) / I_{open}(\lambda)$ and $\eta_r(\lambda) = I_{rNHA}(\lambda) / I_{short}(\lambda)$, respectively. Considering the fact that the incident light must be transmitted, reflected, or absorbed, the normalized absorbance spectrum $\eta_a(\lambda)$ was calculated as $\eta_a(\lambda) = 1 - \eta_t(\lambda) - \eta_r(\lambda)$. The sample was illuminated with a built-in tungsten lamp in the effective wavelength range from 450 to 750 nm.

Figure 6 shows the absorption spectra of four configurations. As shown in Fig. 6(a), the spectra of SQ-hex-VSBPEC, SQ-hex-CP, and SQ-hex-CPPEC were similar. This suggests that these NHAs were identically fabricated. Also, the spectrum of SQ-hex-VSB showed the lowest absorbance and its shape was different from those of the other three configurations, suggesting that the hole size was different. The absorption spectra were also similar for O-sq-VSB and O-sq-VSBPEC and for Tri-hex-VSBPEC and Tri-hex-CPPEC. This suggests that these samples were also identically fabricated.

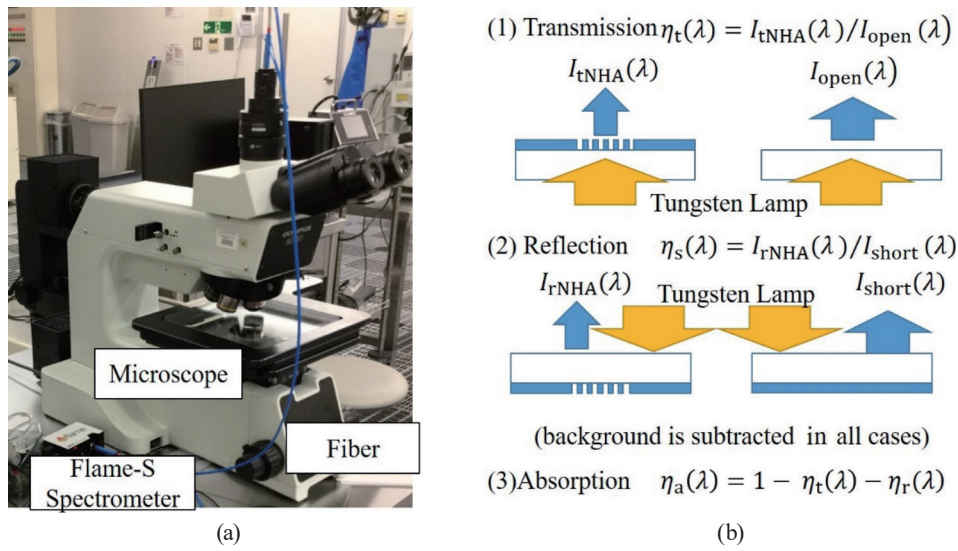


Fig. 5. (Color) Absorption spectral measurement: (a) setup and (b) principle.

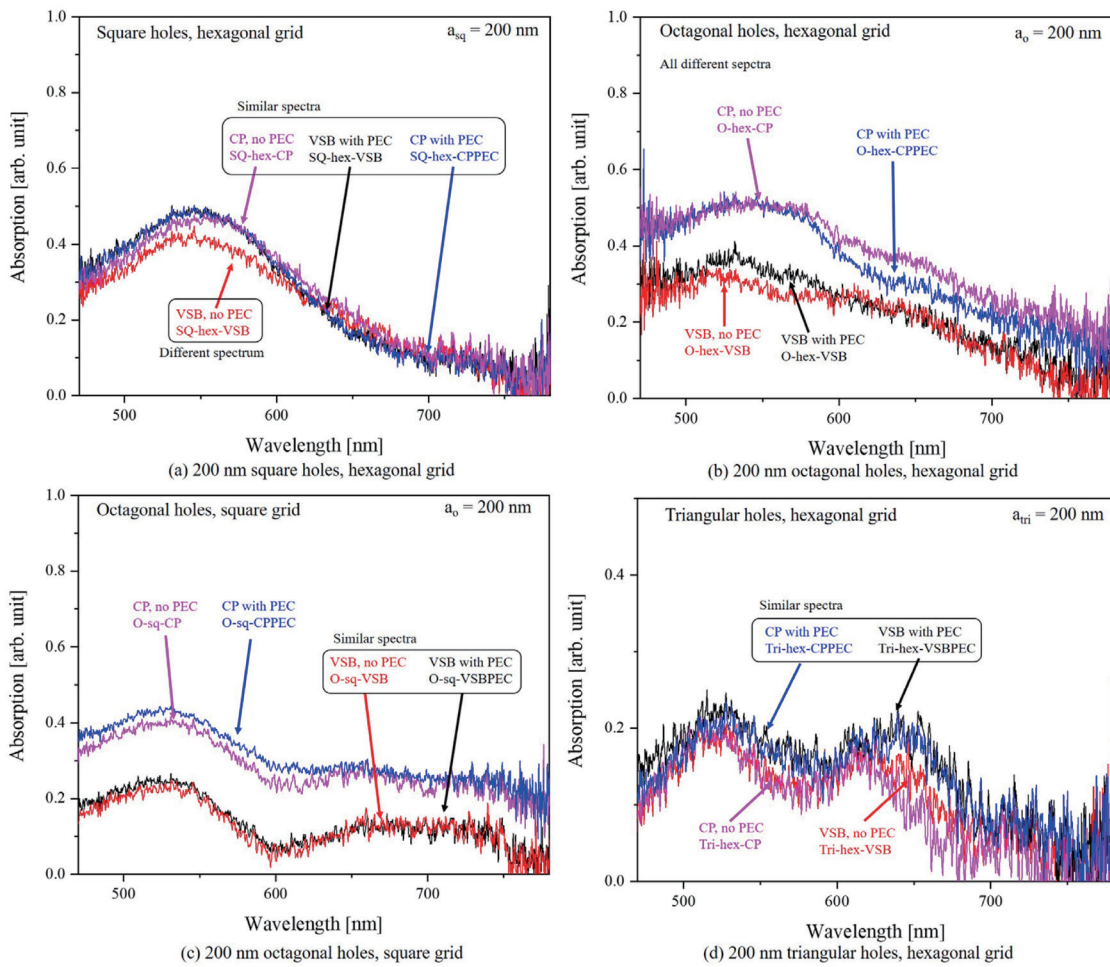


Fig. 6. (Color) Obtained absorption spectra for NHA samples.

3.4 Validation of absorption spectrum dependence on NHA pattern

To confirm the similarity of the NHA patterns, we observed the topography of the Al surface in the noncontact atomic force microscopy mode of scanning probe microscopy (SPM, L-Trace II, Hitachi High-Technologies Corporation). Figures 7–10 show the NHAs of the square-hex, octagonal-hex, octagonal-square, and triangular-hex configurations, respectively. The measurement location was approximately the center of each NHA. As shown in Figs. 7(b)–7(d), the sizes of the NHAs for (b) SQ-hex-VSBPEC (194 nm), (c) SQ-hex-CP (194 nm), and (d) SQ-hex-CPPEC (191 nm) were in good agreement, but (a) SQ-hex-VSB had a different size. Therefore, the optical absorption spectra and NHA sizes were in good agreement. Also, O-sq-VSB [Fig. 9(a), 181 nm] and O-sq-VSBPEC [Fig. 9(b), 180 nm], and Tri-hex-VSBPEC [Fig. 10(b), 175 nm] and Tri-hex-CPPEC [Fig. 10(d), 176 nm] were similar. These results show that the agreement of optical spectra can be a good indicator for verifying that nanopatterns are identically fabricated. This is a critical advantage for process control because an expensive microscopy apparatus is not required.

3.5 Qualitative analyses of shape obtained by VSB and CP methods and PEC

The images in (a) and (b) of Figs. 7–10 show VSB-exposed NHAs and those in (c) and (d) show CP-exposed NHAs. The VSB patterns were approximated by 10-nm-high rectangles and

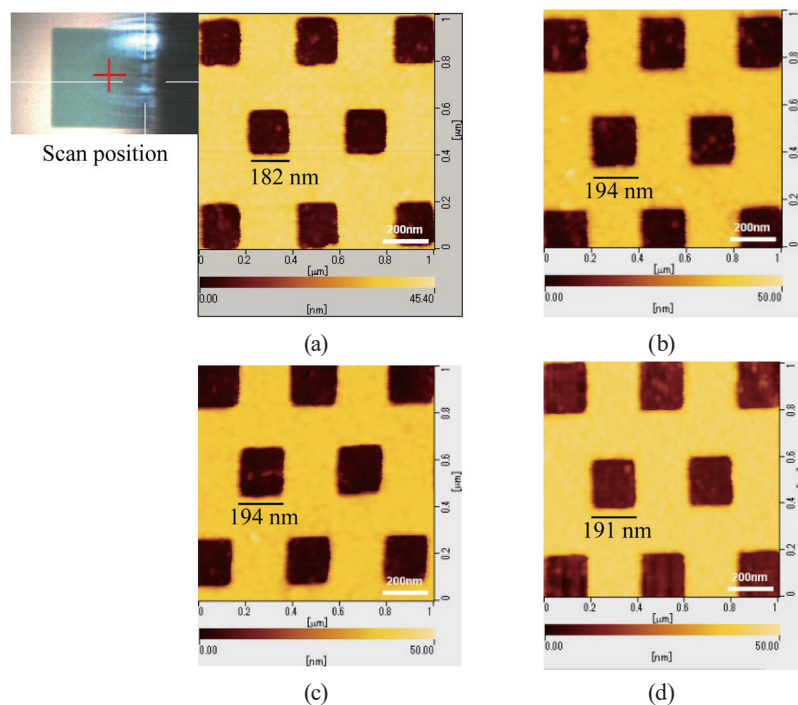


Fig. 7. (Color online) SPM images of hexagonal grid of 200 nm square holes at center of exposed area: (a) VSB without PEC, SQ-hex-VSB, (b) VSB with PEC, SQ-hex-VSBPEC, (c) CP without PEC, SQ-hex-CP, and (d) CP with PEC, SQ-hex-CPPEC. (b)–(d) are identical. The period of each pattern was 400 nm.

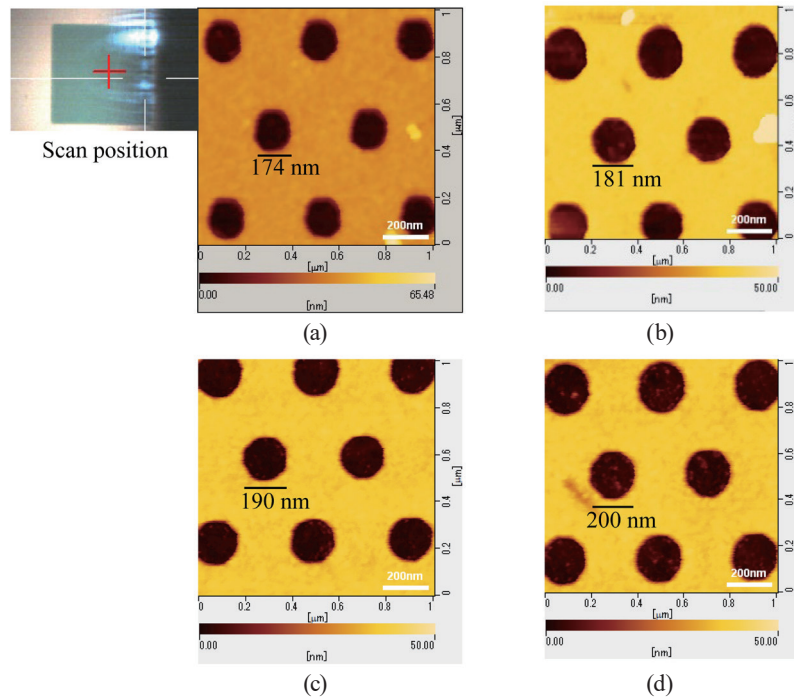


Fig. 8. (Color online) SPM images of hexagonal grid of 200 nm octagonal holes at center of exposed area: (a) VSB without PEC, O-hex-VSB, (b) VSB with PEC, O-hex-VSBPEC, (c) CP without PEC, O-hex-CP, and (d) CP with PEC, O-hex-CPPEC. All NHAs are different. The period of each pattern was 400 nm.

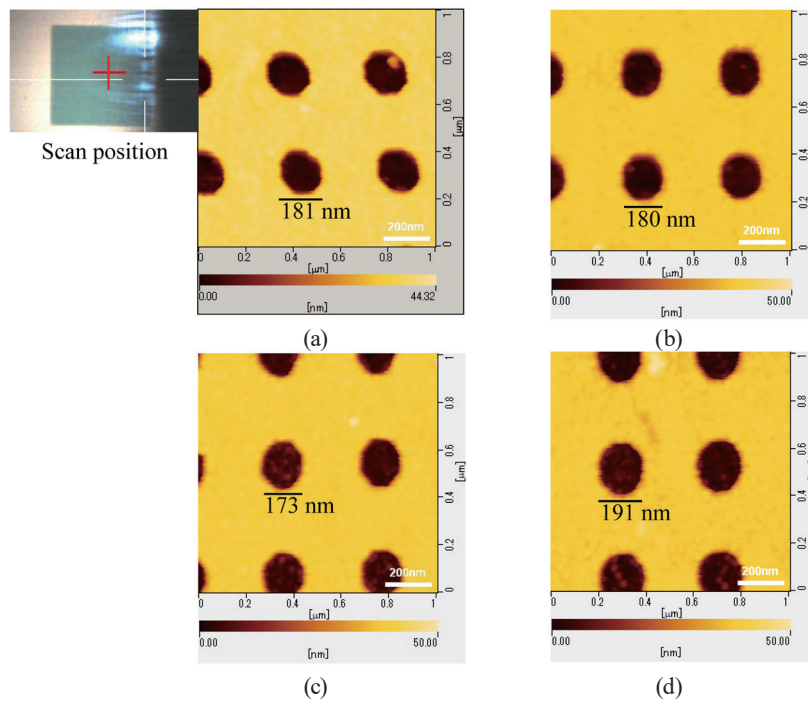


Fig. 9. (Color online) SPM images of square grid of 200 nm octagonal holes at center of exposed area: (a) VSB without PEC, O-sq-VSB, (b) VSB with PEC, O-sq-VSBPEC, (c) CP without PEC, O-sq-CP, and (d) CP with PEC, O-sq-CPPEC. (a) and (b) are identical. The period of each pattern was 400 nm.

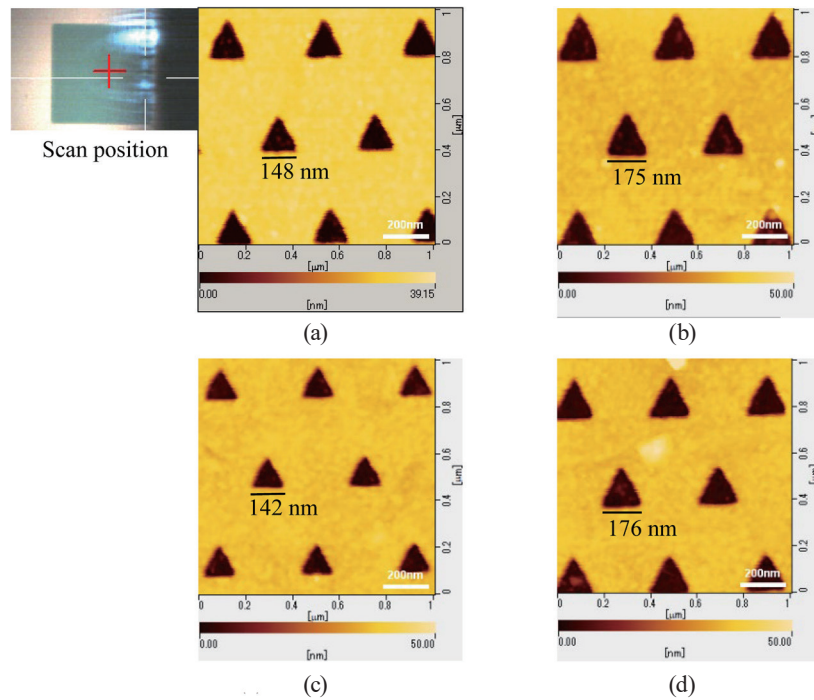


Fig. 10. (Color online) SPM images of hexagonal grid of 200 nm triangular holes at center of exposed area: (a) VSB without PEC, Tri-hex-VSB, (b) VSB with PEC, Tri-hex-VSBPEC, (c) CP without PEC, Tri-hex-CP, and (d) CP with PEC, Tri-hex-CPPEC. (b) and (d) are identical. The period of each pattern was 400 nm.

variable-length shots. Although it is difficult to quantify the pattern size distribution, the VSB patterns seem slightly bumpier than the CP patterns. This difference was clearest for triangular NHAs (Fig. 10).

The effect of PEC was also clearest for triangular NHAs. Without PEC, the realized hole size was 50 nm (25%) smaller than the designed value (200 nm). With PEC, the dose was corrected to 1.4 \times , resulting in a smaller size discrepancy (–25 nm: –12.5% for 200 nm). The fact that we obtained larger NHAs using a higher dose agrees with the fact that we used a positive EB resist.

3.6 Benchmarking NHA evaluation methods

Another standard method of evaluating NHAs is SEM observation. Figure 11 shows SEM (S-4700, Hitachi High-Technologies Corp.) images of the center of SQ-hex-VSB, O-hex-VSB, O-sq-VSB, and Tri-hex-VSB drawn by the VSB method. The substrate is dielectric, causing the edge of each pattern to blur and making the exact location of the pattern edge unclear. In general, one of the reasons of the low resolution of SEM is the actual EB diameter being effectively increased by EB irradiation of a large pattern area including NHA edges. In our case of SEM observation, we considered the charge-up phenomenon; in fact, charge-up also occurred in SPM, and during the scanning operation, the images sometimes shifted. This was

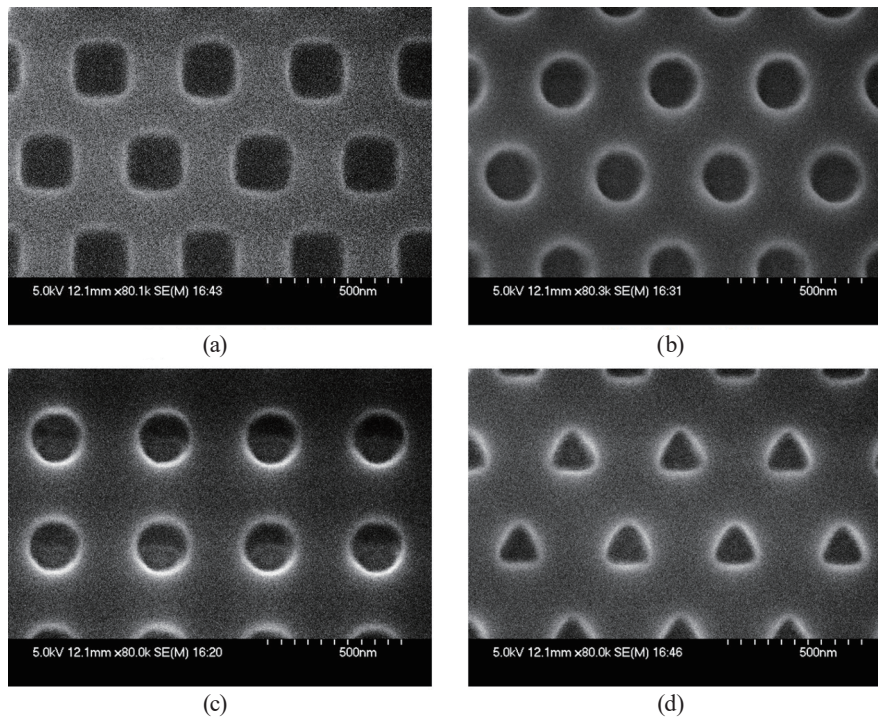


Fig. 11. SEM images of holes obtained by VSB method: (a) square holes in hexagonal grid, SQ-hex-VSB, (b) octagonal holes in hexagonal grid, O-hex-VSB, (c) octagonal holes in square grid, O-sq-VSB, and (d) triangular holes in hexagonal grid, Tri-hex-VSB. The period of each pattern was 400 nm.

Table 2
Comparison of methods.

Method	Information	Charge-up	Apparatus	Purpose
SEM/SPM	Localized shape	Susceptible	Expensive	Analyses
Optical spectra	Averaged	Immune	Inexpensive	Monitoring

due to electric charge-up on the nonconductive (quartz) surface. Figure 9(a) shows a typical example of an SPM image that was transformed as a result of charge-up. Once charge-up occurred, it was necessary to remove the sample from the sample stage and set the apparatus to the neutralization setting for about 1 h. Also, there is a tradeoff between the resolution and the view area. Therefore, we can conclude that SEM and SPM are very useful methods for observing the surface locally, but it is not so simple to extend their results to large-area patterns. In contrast, our proposed optical absorption spectrum method allows us to verify the overall uniformity of NHAs, using only a standard microscope and an inexpensive spectrometer. Its drawbacks are as follows: (1) we cannot observe point defects and (2) it is not straightforward to analytically confirm the measured spectra by first-principles calculation or simulation. As summarized in Table 2, SEM/SPM measurement might be susceptible to charge-up on the nonconductive surface, but our proposed optical method can overcome this problem.

4. Conclusions

Methods of fabrication nanohole patterns having oblique shapes by EBL were benchmarked. A 40-nm-thick Al film nanohole array was fabricated. Smoother slanted patterns were obtained by the CP method than by the VSB method. PEC was shown to be efficient for obtaining shapes closer to the design. Charge-up was found to impede the precise measurement of nanopatterns on glass substrates by both SEM and SPM. As an alternative method, the measurement of optical light absorption spectra was proposed. The spectra were found to be sensitive to variations in pattern size, therefore, making it useful for pattern identity verification without using microscopy methods such as SEM and SPM.

Acknowledgments

This work was supported by the MEXT Nanotechnology Platform. SPM was performed using the apparatus of the University of Tokyo Institute of Innovation, School of Engineering's Nanotechnology Platform Advanced Characterization Platform. All the other processes were performed in the University of Tokyo VDEC Nanotechnology Platform Nanofabrication Center at Takeda Sentanchi Supercleanroom. The invaluable support of the VDEC, University of Tokyo, and Faculty of Engineering cleanroom support team is especially acknowledged. JSPS Kakenhi 16H04345 and French ANR-15-CE33-0022 grants are acknowledged.

References

- 1 R. Ikeno, S. Maruyama, Y. Mita, M. Ikeda, and K. Asada: *J. Micro/Nanolithogr. MEMS MOEMS* **15** (2015) 31606. <https://doi.org/10.1117/1.JMM.15.3.031606>
- 2 A. Higo, T. Sawamura, M. Fujiwara, E. Ota, A. Mizushima, E. Lebrasseur, T. Arakawa, and Y. Mita: *Proc. 32nd IEEE Int. Conf. Microelectronic Test Structures* (2019).
- 3 T. W. Ebbesen, H. J. Lezec, F. Ghaemi, T. Thio, and P. A. Wolf: *Nature* **391** (1998) 667. <https://doi.org/10.1038/35570>
- 4 A. Degiron and T. W. Ebbesen, *J. Opt. A: Pure Appl. Opt.* **7** (2005) S90. <https://doi.org/10.1088/1464-4258/7/2/012>
- 5 C. Genet and T. W. Ebbesen: *Nature* **445** (2007) 39. <https://doi.org/10.1038/nature05350>
- 6 H. Liu and P. Lalanne: *Nature* **452** (2008) 728. <https://doi.org/10.1038/nature06762>
- 7 N. Ikeda, D. Tsuya, Y. Sugimoto, Y. Koike, K. Asakawa, A. Miura, D. Inoue, T. Nomura, H. Fujikawa, and K. Sato: *Proc. Int. Symp. Photonic and Electromagnetic Crystal Structures VIII, 2009*. <https://doi.org/10.1109/omems.2009.5338615>
- 8 D. Inoue, T. Nomura, A. Miura, H. Fujikawa, K. Saito, N. Ikeda, D. Tsuya, Y. Sugimoto, Y. Koike, and K. Asakawa: *Proc. IEEE Conf. Optical MEMS and Nanophotonics* (2009) 150. <https://doi.org/10.1063/1.3560467>
- 9 D. Inoue, A. Miura, T. Nomura, H. Fujikawa, K. Sato, N. Ikeda, D. Tsuya, Y. Sugimoto, and Y. Koide: *Appl. Phys. Lett.* **98** (2001) 093113. <https://doi.org/10.1063/1.3560467>
- 10 <https://genisys-gmbh.com/web/products/beamer.html> (accessed 5th March 2019).
- 11 G. P. Watson, L. A. Fetter, and J. A. Liddle: *J. Vac. Sci. Technol. B* **15** (1997) 2309. <https://doi.org/10.1116/1.589635>
- 12 M. G. R. Thomson: *J. Vac. Sci. Technol. B* **11** (1993) 2768. <https://doi.org/10.1116/1.586599>

About the Authors



Akio Higo received his B.E. degree from Seikei University, Tokyo, Japan, in 2002 and his M.E. and Ph.D. degrees from the Department of Electrical Engineering, The University of Tokyo, Tokyo, Japan, in 2004 and 2007, respectively. From 2007 to 2012, he was an assistant professor at the Research Center for Advanced Science and Technology, and from 2012 to 2016, he was an assistant professor at the World Premier Initiative Advanced Institute for Materials Research, Tohoku University, Sendai, Japan. Since 2017, he has been a project lecturer at the D2T research division, VLSI Design and Education Center, The University of Tokyo. His research interests are in NEMS/MEMS, nanolithography for III-V materials and silicon, and silicon photonics. (higo@if.t.u-tokyo.ac.jp)



Tomoki Sawamura was born in 1970 in Hiroshima Prefecture and graduated from Hiroshima Institute of Technology Polytechnic in 1992. From 1992 to 2004 he worked at Sony LSI Design Inc., where he was involved in SoC LSI device planning, design, and mass production. After working on the development of ultrahigh-throughput Ethernet devices at OA Laboratory Co., Ltd., he was appointed as a MEXT nanotechnology researcher at UTokyo VDEC in 2007, and then as a technician in the School of Engineering. He is currently a technical specialist of the Institute of Engineering Innovation, School of Engineering, The University of Tokyo. He is the engineer responsible for the installation of the F7000S-VD02 EB writer. He is also a MEXT nanotechnology platform expert engineer.



Makoto Fujiwara received his B.A. degree from The University of Tokyo, Japan, in 1977. From 1978 to 2001, he worked in the semiconductor industry. From 2002 to 2015, he worked in software engineering at an independent company. Since 2015, he has been a project researcher at Nanotechnology Platform at VDEC, The University of Tokyo.



Eric Lebrasseur received his B.S. degree in mathematics and his M.S. degree, and Ph.D. degree in physics from the University of Lyon I, France, in 1991, 1993, and 1998, respectively. In 1999, he started to work in the field of MEMS at The University of Tokyo in Japan as a postdoctoral research fellow. Since then, he has been involved in the design and fabrication of MEMS at various companies and institutes in France (Memscap in Grenoble, Femto-ST in Besançon) and UTokyo. Since 2012, he has been a project researcher as part of the Nanotechnology Platform Japan at UTokyo VDEC. He is a MEXT nanotechnology platform expert engineer. (eric@if.t.u-tokyo.ac.jp)



Ayako Mizushima received her B.S. degree from Yokohama National University in 1996 and her M.S. degree from Yokohama National University in 1998, both in chemical engineering. From 1998 to 2008 she worked at Sumitomo Bakelite Co., Ltd. as a researcher of photosensitive resins for semiconductor. From 2009 to 2016, she worked as a process engineer at Professor Motoichi Ohtsu Lab in The University of Tokyo. Since 2016, she has been a member of the Nanotechnology Platform Japan. She is a MEXT nanotechnology platform expert engineer.



Etsuko Ota received her B.S. degree in electrical engineering from Ibaraki University, Japan, in 1985. From 1985 to 1988, 1996 to 1998, and 1999 to 2001, she worked on the development of a stepper system at Nikon Corporation, Japan and during 1989 to 1993, she worked at Nikon Precision Europe GmbH (Germany). From 2008 to 2016, she was a research assistant at The University of Tokyo. Since 2016, she has been a member of the Nanotechnology Platform Japan. Her research interests are in microfabrication, surface analysis, and sensors. She is a MEXT nanotechnology platform senior engineer. (ohta@if.t.u-tokyo.ac.jp)



Yoshio Mita is an associate professor of the Department of Electrical Engineering and Information Systems, Graduate School of Engineering, The University of Tokyo (UTokyo). He obtained his B.E. (1995), M.E. (1997), and Ph.D. (2000) degrees from the Department of Electrical and Electronic Engineering, UTokyo. He served as an assistant professor of VLSI Design and Education Center (VDEC), UTokyo, and was promoted to a lecturer in the Department of Electrical Engineering in 2001 and then to an associate professor in 2005. Since 2012, Dr. Mita has been a manager of the Ministry of Education (MEXT)-supported National Nanotechnology Platform UTokyo open nanofabrication site, operated jointly by VDEC and the Faculty of Engineering. His research interests include CMOS and MEMS integration technologies, such as high-voltage-generating photovoltaics for autonomous distributed microsystems. (mems@if.t.u-tokyo.ac.jp)